Magnetization and structure of ultrathin Fe films

R. Zdyb,[1,2] T. O. Menteş,[3] A. Locatelli,[3] M. A. Niño,[3] and E. Bauer[1]
[1]*Department of Physics, Arizona State University, Tempe, Arizona 85287-1504, USA*
[2]*Institute of Physics, Maria Curie-Sklodowska University, 20-031 Lublin, Poland*
[3]*Sincrotrone Trieste, S.C.p.A., Basovizza, Trieste 34012, Italy*
(Received 28 July 2009; revised manuscript received 18 September 2009; published 23 November 2009)

The connection between magnetization and structure of ultrathin films is studied at room temperature for the case of Fe films on W(110) by inserting a 2-monolayer-thick growth-modifying Au layer between film and substrate using spin-polarized low-energy electron microscopy and low-energy electron diffraction. Ferromagnetic order with the easy axis pointing in the $[1\bar{1}0]$ direction appears upon percolation at 1.6 monolayers. Shortly thereafter, the easy axis rotates into the [001] direction. With further increasing thickness the magnetization oscillates between the [001] and the $[1\bar{1}0]$ direction with a maximum deviation from the [001] direction at seven monolayers where the magnetic signal has a maximum. The changes in the magnetization are associated with changes in the structure, strain, and morphology that are deduced from the diffraction patterns and which strongly influence the competition between interface anisotropy, magnetoelastic anisotropy, and dipolar surface anisotropy.

DOI: 10.1103/PhysRevB.80.184425 PACS number(s): 75.30.Gw, 68.35.Ct, 68.37.Nq, 75.70.Ak

I. INTRODUCTION

Ultrathin ferromagnetic metal films attract considerable attention for both fundamental and practical reasons.[1] One of their most interesting features is the magnetization direction which usually differs from that in the bulk. It is determined by the interplay of several anisotropies among which interface anisotropy plays a significant role inducing in many cases a perpendicular easy axis.[2] Another important anisotropy which strongly influences the easy axis direction and is always present in ultrathin films grown by heteroepitaxy on rigid substrates is the magnetoelastic anisotropy. It is due to the strain that develops in the film, which is usually caused by the lattice misfit between the growing layer and the substrate. The direction of the easy axis changes often with film thickness, temperature, or coverage by other elements on top of the layer, which change the relative contributions of the various anisotropies.[2] In this paper we show that the relative contributions can also be considerably modified by inserting a thin interlayer between the substrate and the growing film. We use for this purpose one of the most studied systems, Fe on W(110), and Au as interlayer material.

Fe films on W(110) are pseudomorphic (ps) up to 1.2–1.8 monolayer (ML) depending on deposition temperature.[3–5] With increasing thickness the Fe layer transforms into the bulk bcc crystallographic structure. Starting at about 1.2 ML, the strain in the layer, caused by the lattice misfit of 10.4%, is released by a one-dimensional (1D) lattice of misfit dislocations running along the [001] direction.[3] At about 2 ML the 1D lattice transforms into a two-dimensional (2D) lattice of misfit dislocations, which produces well-developed low-energy electron diffraction (LEED) patterns with additional diffraction spots surrounding the integer order Fe spots.[3] According to scanning tunneling microscopy (STM) studies additional rows of Fe atoms are incorporated along the $\langle 11\bar{1}\rangle$ directions in the 2D dislocation network.[5] In STM the 2D network is visible in films as thick as 13 ML.[6] The periodicities associated with the distortions were reported to be 33.4 Å and 37.1 Å (Ref. 5) or 35.84 Å and 50.76 Å (Ref. 6) in the [001] and $[1\bar{1}0]$ directions, respectively.

While 2-ML-thick islands surrounded by a continuous 1-ML-thick film are perpendicularly magnetized,[7] the magnetization points in the in-plane $[1\bar{1}0]$ direction from 1-ML-thick islands up to about 50 ML.[8,9] Then a spin reorientation transition (SRT) occurs and the magnetization rotates into the easy axis direction of bulk Fe ([001]), which is determined by the magnetocrystalline anisotropy.[8] Originally, the surface/interface anisotropy energy density has been made responsible for the direction of the easy axis below 50 ML.[8,9] This explanation has been supported later by the observation that Au, Ag, and oxygen overlayers have a strong influence on the thickness at which the SRT occurs.[10] Another explanation, based on film-substrate cantilever bending measurements of the stress[11] and on x-ray diffraction measurements of the strain,[6] attributes the $[1\bar{1}0]$ easy axis to magnetoelastic anisotropy.

On the Au(111) surface and thick epitaxial (111)-oriented Au films Fe grows initially pseudomorphically, that is, in a highly strained fcc structure, up to about 2 ML,[12] 3 ML,[13–17] 4 ML,[18] or 5 ML,[19] despite the large misfit (−13.6%). In this thickness range the magnetization points out of plane[15–17,20–22] apparently due to the high Fe/Au out-of-plane magnetic interface anisotropy energy density.[23] Above this thickness the film converts into the bcc structure and the easy axis rotates in plane.

On a 10 ML Au/W(110) substrate the Fe layer is pseudomorphic with out-of-plane magnetization up to 2.7 ML. At this thickness, it transforms into the bcc structure in which the magnetization points into the in-plane [001] direction.[24] This SRT has been attributed to the magnetoelastic anisotropy caused by film strain. In the Fe $[1\bar{1}0]$ direction, which is parallel to the Au $[11\bar{2}]$ direction, the strain is about 23%; in the Fe[001] direction it is 0.6%. Because of the small misfit in the [001] direction the Fe lattice locks in this direction into the Au lattice and builds up considerable strain with

increasing thickness. In the $[1\bar{1}0]$ direction the Fe lattice is floating on the Au(111) surface because of the large lattice mismatch. The situation is completely different on thinner Au overlayers on W(110). On 1 ML Au the easy axis is the $[1\bar{1}0]$ direction up to the largest thickness studied (6 ML); on 3 and 4 ML it points from the onset of magnetization in the [001] direction.[25]

In the present paper we report the results for Fe layers grown on a 2 ML Au/W(110) substrate. This system shows in more detail the influence of a structure-modifying interfacial layer on the magnetization of ultrathin layers. It has features that are similar to those observed in Fe grown on both W(110) and Au(111) substrates. On the one hand, the easy axis is initially in plane in the $[1\bar{1}0]$ direction as on the W(110) substrate. On the other hand, it rotates into the [001] direction as on the bulk Au(111) substrate but already at 2 ML Fe. However, contrary to bulk Au(111) substrates and thick Au layers on W(110) or other substrates no out-of-plane magnetization was found.

II. EXPERIMENTAL

The experiments were performed in two low-energy electron microscope (LEEM) instruments. All magnetic and part of the structural measurements were done with a spin-polarized low-energy electron microscope (SPLEEM). The detailed crystallographic structure of the Fe films was studied with LEED in a spectroscopic photoemission and low-energy electron microscope (SPELEEM) instrument.[26,27] Both instruments work under ultrahigh vacuum conditions with a base pressure in the high 10^{-11} mbar (SPLEEM) and low 10^{-10} mbar (SPELEEM) range. The SPLEEM microscope is a conventional LEEM microscope equipped with a spin-polarized electron gun and a spin manipulator that allows rotation of the polarization vector of the electron beam in any direction.[28,29] In order to obtain a magnetic image two images with opposite electron beam polarization vector, I_{up} and I_{down}, are recorded with the spin polarization vector **P** pointing in three crystallographic directions: parallel to the in-plane $[1\bar{1}0]$ and [001] directions and to the out-of-plane direction [110] of W. Then the asymmetry parameter $A_{\mathrm{ex}}=(I_{\mathrm{up}}-I_{\mathrm{down}})/(I_{\mathrm{up}}+I_{\mathrm{down}})$ is calculated pixel by pixel for each **P** direction and the resulting values are displayed as a magnetic image. The image subtraction removes all features that are spin independent. Only the magnetic contribution to the image remains.

The W(110) substrate was cleaned in the standard way by heating in oxygen at about 1400 K and then removing the remaining oxide layer by several flashes up to about 2000 K. The substrate cleanness was controlled with LEED and checked via the step flow growth of Au at elevated temperature, which is very sensitive to contamination. First two monolayers of gold were deposited at 600 K and then the substrate was allowed to cool to room temperature (RT). Then Fe was deposited on top of this 2 ML Au/W(110) substrate at RT. In the SPELEEM instrument the depositions were started at several substrate temperatures in order to examine the temperature influence. Annealing experiments were performed as well.

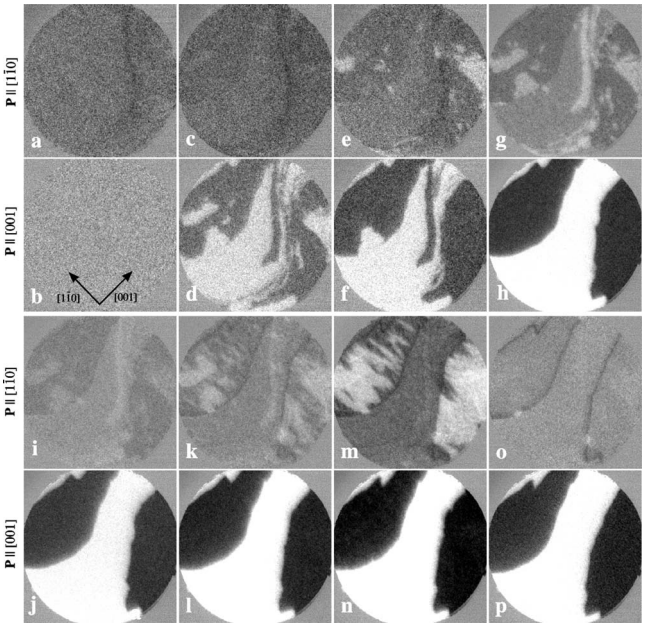

FIG. 1. SPLEEM images taken with polarization parallel to the $[1\bar{1}0]$ direction (first and third rows) and parallel to the [001] direction (second and fourth rows) of the W(110) surface during growth of the Fe layer on 2 ML Au/W(110) at room temperature. Film thickness in monolayers: [(a), (b)] 1.60, [(c), (d)] 1.67, [(e), (f)] 1.72, [(g), (h)] 1.84, [(i), (j)] 2.48, [(k), (l)] 4.67, [(m), (n)] 6.1, and [(o), (p)] 11.9. The crystallographic directions of the W substrate are indicated in (b). Field of view 14 μm, electron energy 3.5 eV.

Both Au and Fe were deposited from resistively (SPLEEM) and e-beam (SPELEEM) heated crucibles with rates of about 0.13 and 0.1 ML/min, respectively. During the depositions the pressure increased to about 5×10^{-10} mbar. The iron thickness was calibrated via the time necessary to complete one pseudomorphic (ps) monolayer of Fe on the bare W(110) surface at elevated temperature. The completion of the ps monolayer is visible as a strong contrast change in the LEEM image. The accuracy of this thickness calibration is $\pm5\%$. The thickness is measured in ML units corresponding to the packing density of the Fe(110) plane in the bulk (17.21×10^{14} atoms/cm^2). In these units 1 ps ML$\approx$0.82 ML.

The reciprocal space distances were calibrated with the distances between the diffraction spots of the bare W(110) surface. The diffraction patterns of the 2 ML Au/W(110) system were the same as those in Ref. 30 with exactly the same lattice constants.

III. RESULTS

Magnetism

Figure 1 shows a typical series of SPLEEM images recorded during the growth of Fe on the 2 ML Au/W(110) substrate at room temperature. Figures 1(a) and 1(b) show magnetic images recorded just after the onset of magnetization which occurs at 1.6 ML. With $\mathbf{P}\|[1\bar{1}0]$ huge domains appear with sizes of the order of millimeters and weak mag-

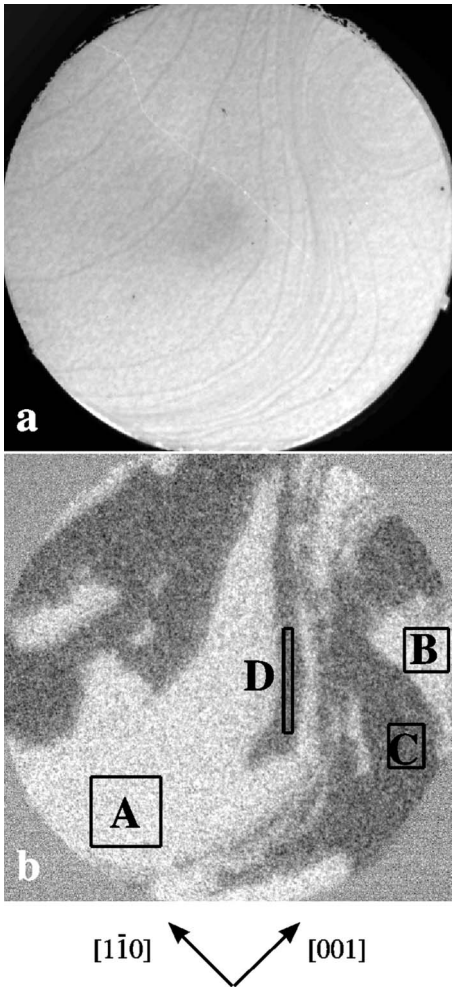

FIG. 2. LEEM (a) and SPLEEM (b) images of 1.7 ML Fe on 2 ML Au/W(110). Field of view 14 μm, electron energy 3.5 eV. The crystallographic directions of the W substrate are indicated at the bottom.

netic contrast [Fig. 1(a)]. When **P** is parallel to [001] [Fig. 1(b)] no magnetic contrast is seen. Thus, the magnetization **M** is purely parallel to [1$\bar{1}$0]. Just after the onset, at 1.67 ML, the huge [1$\bar{1}$0] domains break up into smaller domains with considerable magnetic contrast in the [001] direction [Fig. 1(d)].

The smaller domains are connected to some extent with the substrate morphology. For example, the narrow long domain in vertical direction [Fig. 1(d)] is located at a step bunch as seen in the LEEM image [Fig. 2(a)]. The contrast ratio of the [1$\bar{1}$0] and [001] images changes rapidly with increasing thickness [Figs. 1(e)–1(j)] indicating rapid rotation of **M** from [1$\bar{1}$0] to [001]. At 2.0 ML (not shown) there is nearly no contrast in the [1$\bar{1}$0] direction: **M** is nearly parallel to [001] between 2 and 4 ML [Figs. 1(i) and 1(j)]. Above 4 ML the contrast in the [1$\bar{1}$0] direction increases again, initially with the same domain distribution as below 2 ML [Figs. 1(k) and 1(l)]. With further increasing thickness some of the domains in the [1$\bar{1}$0] direction break up into subdomains elongated in the [1$\bar{1}$0] direction [Figs. 1(k) and 1(m)]. Simultaneously the overall contrast increases. Finally above 7 ML the contrast in the [1$\bar{1}$0] azimuth decreases again and at 12 ML it is nearly zero as seen in Fig. 1(o) which shows clear domain wall contrast. Thus, **M** is now nearly parallel to [001]. At no thickness out-of-plane contrast (images with **P**$\|$[110]) is observed.

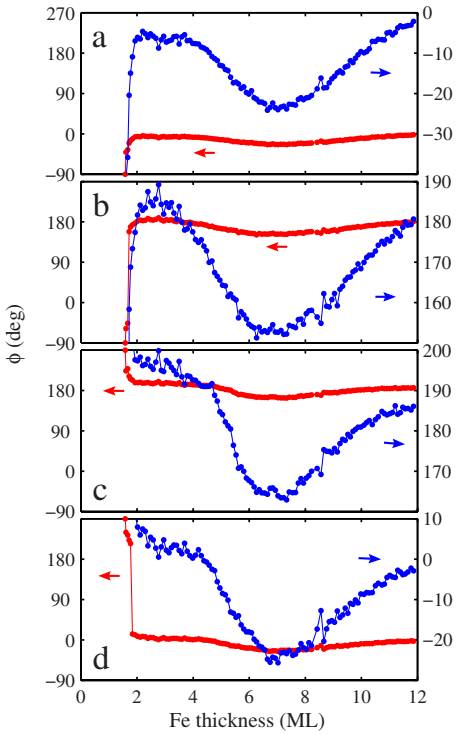

FIG. 3. (Color online) Direction of the magnetization as a function of thickness in the four domains indicated in Fig. 2. (a) domain A, (b) domain B, (c) domain C, and (d) domain D. Magnified ϕ curves are shown in blue with right axis. The angle ϕ is measured from the W[001] direction. ϕ=270° is equivalent to ϕ=−90°.

The evolution of the magnetization with increasing thickness can be seen in more detail by plotting the ratio of gray levels of the asymmetry images taken in the [1$\bar{1}$0] and in the [001] direction. This gives the tangent of the angle of the magnetization with respect to the [001] axis. This angle is shown for a few selected domains in Fig. 3. They are indicated in Fig. 2(b) by A–D. The corresponding asymmetry values, which do not differ significantly from domain to domain—except for the domain in the step bunch region [D in Fig. 2(b)], where the asymmetry is about 10% lower—are shown in Fig. 4. While in the larger regions **M** rotates to the nearest [001] direction (A and C), in smaller regions it flips after initial rotation into the opposite [001] direction (B and D), apparently driven by the elimination of 180° domain walls with the larger domains. In the elongated subdomains visible in Fig. 1(m) the [1$\bar{1}$0] component of **M** points in opposite directions. Because of the dominating [001] component of **M** the angle between the subdomains is small. It reaches a maximum value of 60° at 7 ML and then decreases again. At 10 ML it is still 25°; however, the domains are not elongated any longer but appear only as weak background in the otherwise large domains. In all domains the asymmetry

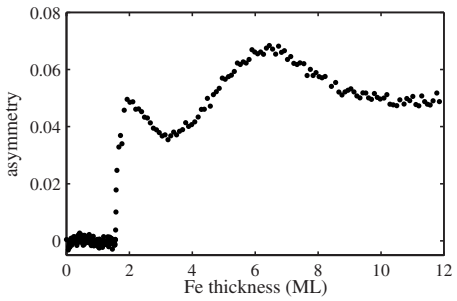

FIG. 4. Total asymmetry (vector-summed) as a function of thickness. Because the low degree of polarization of the electron beam (20%–25%) the true asymmetry is by a factor of 4–5 larger.

increases initially rapidly up to 2 ML followed by a sharp decrease to 3.5 ML. Subsequently it rises slowly to 6.5 ML from where it slowly decreases up to the highest coverages. As will be seen in the next section, these changes are closely connected with structural changes.

Structure, strain, and morphology

Figure 5 shows LEED patterns recorded during the initial growth of Fe on the 2 ML Au/W(110) substrate at room temperature. The LEED pattern of the 2 ML Au/W(110) substrate [Fig. 5(a)] shows strong satellite spots around the W spots caused by double scattering and misfit dislocations. It is due to two Au(111) domains whose $[11\bar{2}]$ directions deviate by $\pm 2.3°$ from the $[1\bar{1}0]$ direction of the W(110) substrate.[30] The 2.3° rotation indicates that the Au double layer has the Greninger-Troiano orientation[31] with respect to the substrate. There is also a small intensity asymmetry of the Au spots, mainly with respect to the $[1\bar{1}0]$ direction, but it is not a reliable indication of the 1° misorientation of the fcc (111) plane relative to the bcc (110) plane of the

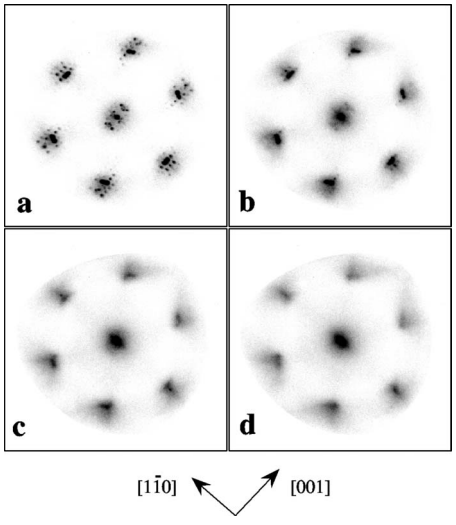

FIG. 5. LEED patterns from the initial growth of a Fe layer on a Au double layer on W(110) at room temperature. Fe film thickness in monolayers: (a) 0, (b) 0.5, (c) 1, and (d) 1.5. Electron energy 30 eV. The crystallographic directions of the W substrate are indicated at the bottom.

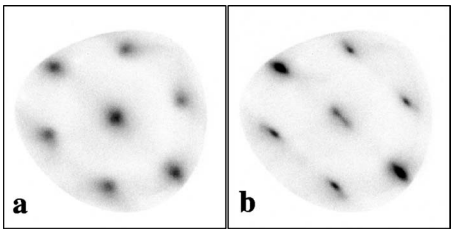

FIG. 6. LEED patterns typical for intermediate thicknesses, here at 6 monolayers (a) and for thicker films, here at 11 monolayers (b). Electron energy 50 eV.

Greninger-Troiano orientation because a slight beam misalignment cannot be excluded.

Deposition of 0.5 ML Fe replaces the double scattering/misfit dislocation spots by diffuse streaked regions [Fig. 5(b)] indicating increasing disorder. At 1 ML Fe [Fig. 5(c)] the Au double spots are barely visible above the diffuse background, the asymmetry of the pattern and the background has further increased, and at 1.5 ML Fe [Fig. 5(d)] the original Au doublet spots are completely replaced by the diffuse streaked regions. Simultaneously with these changes the intensity and sharpness of the strongest satellites of the (00) spot decrease in an oscillatory manner with maximum sharpness at about 1.3 ML. At 2 ML these spots have disappeared. The pattern now has the symmetry of a bcc (110) plane. At about 2 ML the (00) spot elongates in the $[1\bar{1}0]$ direction. At 2.6 ML the elongation develops into two satellites and at 4 ML additional satellites appear. They correspond to a periodicity of 19 times the periodicity of the main spots and are attributed to misfit dislocations. At some energies they are also weakly visible around the integral order spots. This pattern persists up to 8 ML, with maximum intensity and sharpness between 6 and 7 ML.

Above 2 ML diffuse regions inside the W $[1\bar{1}0]$ spot positions develop whose nature will be discussed below. Above 3 ML the intensity of the diffuse streaks radiating from the $\langle 112 \rangle$ spots decreases and diffuse round spots develop as illustrated in Fig. 6(a). The disappearance of the diffuse streaks and the sharpness of the satellite spots indicate that the originally very fine-grained layer has recrystallized into larger well-ordered regions. Above 7 ML the integral order spots become sharper in the [001] direction but develop streaking along the $[1\bar{1}0]$ direction [Fig. 6(b)]. From the full width at half maximum of the spots in the [001] direction an average crystal size of 6.4 nm is obtained. The sharpness and position along the $[1\bar{1}0]$ direction of the streaked spots vary with energy characteristic of faceting. This is the well-known "kinetic" faceting.[32] It persists up to the largest film thickness studied.

The initial growth can be followed in more detail via the intensity of characteristic spots as a function of film thickness. Figure 7(a) shows the decay of the intensity of the Au doublet spots. It can be fitted by a pure exponential, in contrast to the linear decrease $I/I_0 = 1 - \theta \times [1 - \exp(t_{\mathrm{ML}}/\lambda_{ee})]$ expected for initial growth of monolayer islands as observed in the growth of Fe on the (111) surface of bulk Au.[13,14] Here θ is the coverage by monolayer islands, $t_{\mathrm{ML}} \approx 2$ Å the mono-

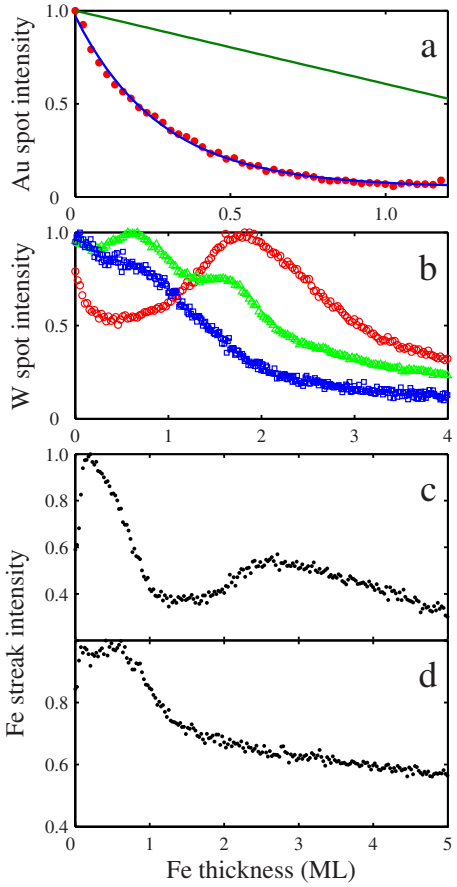

FIG. 7. (Color online) Intensity of characteristic features of the LEED patterns as a function of film thickness normalized to their maximum intensity. (a) Typical dependence of the intensity of the Au double spots. The experimental data are well fitted by an exponential in contrast to the linear dependence expected for monolayer island growth. (b) Intensity of the W spots in the $[11\bar{2}]$ direction. Green triangles: 80 °C; red circles: 40 °C; blue squares: 20 °C. [(c), (d)] Intensity along the diffuse streaks taken close to the W spot (c) and at the position at which the spot of an epitaxial Fe layer is expected (d).

layer thickness, and $\lambda_{ee} \approx 4$ Å the inelastic mean free path. Taking into account that second and third layer islands form on the initial monolayer islands with increasing coverage does not allow fitting the rapid exponential decay. The exponential decrease requires a rapid destruction of the initial LEED pattern by Fe condensation. This process is very temperature sensitive as indicated by the intensity changes of the W (+ ps Au) spots shown in Fig. 7(b) for three temperatures of the start of the deposition, 80 °C (triangles), 40 °C (circles), and 20 °C (squares). At the highest temperature the intensity decays in an oscillatory manner related to the growth of the first two monolayers; at the intermediate temperature it decays initially rapidly but reaches a maximum again close to completion of the second monolayer; and at the lowest temperature it decreases initially slowly, then rapidly up to the second monolayer. These differences are attributed to diffusion-limited structural perfection differences. The intensity of these spots is higher than that of the diffuse streaks and increases strongly relative to them with increasing deposition temperature. The evolution of the diffuse streaks with increasing Fe thickness, clearly seen in Fig. 5(d), is shown in Figs. 7(c) and 7(d) for a region close to and far away from the W spots in the ⟨112⟩ directions along the streaks. While the initial peak is attributed to the disorder connected with the rearrangement of the Au double layer, the maximum between 2 and 3 ML of the outer region in Fig. 7(c) is near the position expected for an epitaxial bcc Fe layer in parallel orientation with respect to W. This will become more evident later in connection with the LEED patterns of annealed films, which will also give an indication of the nature of the diffuse regions inside of the W $[1\bar{1}0]$ spots mentioned above.

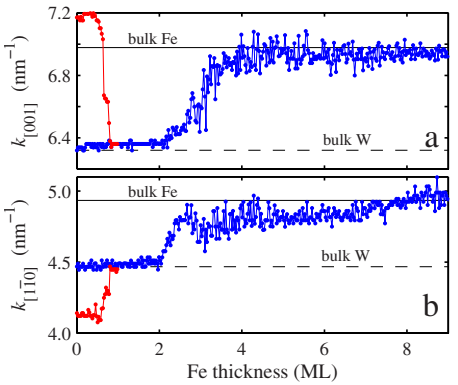

FIG. 8. (Color online) Reciprocal lattice distances as a function of film thickness. (a) in [001] direction; (b) in $[1\bar{1}0]$ direction. The corresponding distances for W (6.32 and 4.47 nm^{-1}) and for Fe in the bulk (6.98 and 4.93 nm^{-1}) are indicated by horizontal broken and solid lines, respectively. Blue: initial W spots; red: Au spots.

The changes in the spot intensities and shapes were accompanied with changes in the spot positions. Results of the changes in the reciprocal lattice distances are shown in Fig. 8 for the [001] direction (a) and the $[1\bar{1}0]$ direction (b). The k value in the [001] direction remains constant at the W value ($2/a_W = 0.632$ Å^{-1}) up to 2 ML and then rises to that of Fe ($2/a_{Fe} = 0.698$ Å^{-1}). In the $[1\bar{1}0]$ direction k is also constant at the W value ($\sqrt{2}/a_W = 0.447$ Å^{-1}) up to 2 ML. Thereafter, it rises initially fast and then slower to the Fe value ($\sqrt{2}/a_{Fe} = 0.493$ Å^{-1}) which it approaches at about 8 ML. The reciprocal lattice distances derived from the Au spot positions are constant up to about 0.5 ML ($[1\bar{1}0]$) or increase slightly ([001]) but thereafter start to approach the W distances while simultaneously rapidly weakening [see Fig. 7(a)]. Depending upon temperature at the beginning of Fe deposition the Au spots merge the W spots between 0.5 and 1.3 ML Fe.

In order to obtain some insight into the structure of the film at small thickness, in which the diffuse streaking dominates, films in these thickness ranges were annealed. Figure 9(a) shows the LEED pattern of an about 2-ML-thick film annealed up to 120 °C. The intensity of all spots depends strongly upon energy which indicates strong double scattering. The interpretation of this pattern is shown in Fig. 9(b). This interpretation suggests that the diffuse streaks along the ⟨112⟩ directions seen before annealing are due to the coex-

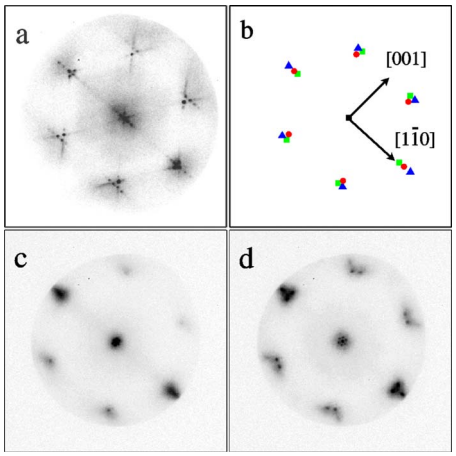

FIG. 9. (Color online) (a) LEED pattern of Fe film annealed up to 120 °C with thickness of about 2 ML; (b) interpretation of pattern (a). Red circles: W; blue triangles: Fe; green squares: Au. All other spots: double scattering. [(c), (d)] Thickness 5 ML before and after annealing up to 120 °C. Electron energy 40 eV.

istence of two structures: bulklike bcc (110)-oriented Fe nanocrystals which are very narrow or disordered in the ⟨112⟩ directions, that is, normal to the close-packed ⟨111⟩ directions, and similarly narrow, slightly distorted (111)-oriented Au, which grow upon annealing sufficiently to produce sharp diffraction spots. The coexistence of the diffuse streaks with the stronger W(+Au) spots shows that the initial layer consists above 0.5–1.3 ML of dominating ps Fe regions with W periodicity and narrow bulklike bcc Fe nanocrystals.

In order to shed light on the diffuse regions inside the W spots along the [1$\bar{1}$0] [Fig. 9(c)] mentioned above a 5-ML-thick film was annealed up to 120 °C, which gave the LEED pattern of Fig. 9(d). The outer spots in the [1$\bar{1}$0] direction are from the Fe layer while the doublet pattern can be attributed to a Au layer with the same lattice constant as that of the Au double layer on W(110) [Fig. 5(a)] but with angle of 7.0° between the two azimuthal orientations instead of 4.6° on W(110). XPS studies of the attenuation of W and Au 4*f* electrons in ultrathin Fe overlayers support the conclusion that a monolayer of Au is on top of the Fe layer.[33]

IV. DISCUSSION

Before comparing the results of the magnetic and structural measurements some aspects of the experimental methods have to be mentioned, which are important for the understanding of these results. First of all, the asymmetry of the magnetic images is not a quantitative measure of the magnetization of the layer for two reasons: (i) multiple scattering and (ii) limited sampling depth. (i) Multiple scattering, which can be taken into account properly by the dynamical theory of electron diffraction, produces contribution to the specularly reflected beam from electrons which have been scattered twice or more into angles different from 180°, for example, twice by 90°. As a consequence, spin-orbit effects also can contribute to the observed spin dependence of the signal. At the low energies used in the SPLEEM studies

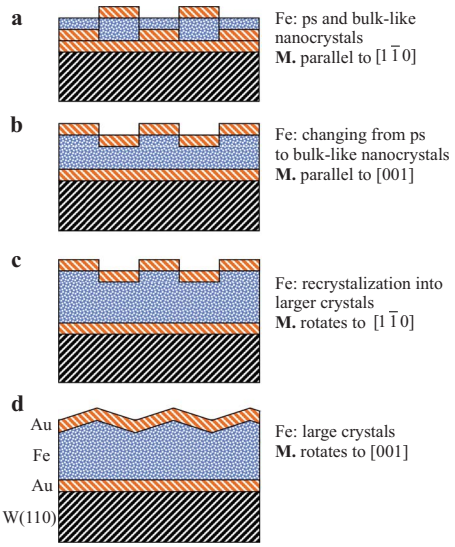

FIG. 10. (Color online) Sketch of model of the growing Fe layer at the onset of ferromagnetic order at 1.6 ML (a), between 2 and 4 ML (b), 4 and 7 ML (c), and above 7 ML (d).

these effects may be small but have to be kept in mind when the asymmetry is small. For example, on the clean W(110) surface, which is nonmagnetic, a small energy-dependent asymmetry is observed.[34] (ii) The sampling depth is limited by the short inelastic mean free path (IMFP). In materials with a high density of unoccupied states above the Fermi level such as in the transition metals, excitations into these states make the IMFP of slow electrons very small,[35] in contrast to metals with closed *d* shells such as Au in which the IMFP rises sharply with decreasing energy. In particular in Fe the IMFP at the energy used in this experiment is only 3 Å and 5 Å for spin-down and spin-up electrons, respectively.[36] As a consequence, the magnetic signal is dominated by the contributions of the top few layers. This has to be kept in mind in connection with the question of noncollinear magnetization, in which the direction of the spin changes with thickness, and when comparing SPLEEM results with magnetic measurements, that average over the film thickness.

In the comparison of magnetism and structure it is useful to consider four regions apparent in the total asymmetry (Fig. 4) and in the reciprocal lattice distances (Fig. 8) separately: less than 2 ML, from 2 to 4 ML, from 4 to 7 ML, and more than 7 ML. In the first region the 2 ML Au structure converts into a pseudomorphic structure. Fe grows pseudomorphically on this layer mixed with very fine-grained Fe crystals. Part of the Au diffuses onto the 2-ML-thick regions of the growing Fe film to form a Au ML on top of them. Figure 10 shows a sketch of the model of the growing Fe layer. The appearance of ferromagnetism at 1.6 ML coincides with the onset of percolation, which is clearly evident in STM studies.[13,14] The direction of the magnetization in this early phase is attributed to the interface anisotropy with the W/Au substrate with W periodicity, which favors this orientation.[25] The rapid change in the direction of **M** from [1$\bar{1}$0] toward [001] coincides with the formation of the Au overlayer on the 2-ML-thick Fe regions. The Au overlayer on

this Fe layer favors [001] as easy axis,[10,37] Fig. 10(b).

At 4 ML the intensity of the diffuse streaks due to Fe nanocrystals has decreased significantly. This, together with the appearance of (00) satellites due to the dislocation network, indicates recrystallization of the nanocrystals. The resulting Fe layer on the W/Au substrate has a structure very similar to that of Fe grown directly on the W substrate but the Au interlayer, very likely only 1 ML thick, causes a slightly different stress in the film. As a consequence, the dislocation network is somewhat different from that on the W surface although the W/Au surface periodicity is the same. Here the periodicity is 19 times the overlayer period; on the W surface it is 12.5 times this period.[6] The different dislocation system is attributed to the stress-reducing effect of the Au underlayer and to the misfit with the Au overlayer, which is also responsible for the [001] easy axis. With increasing film thickness the relative contribution of the Au/Fe interface anisotropy decreases and **M** rotates toward the $[1\bar{1}0]$ direction, Fig. 10(c). Assuming that the interface anisotropies of the two interfaces are constant, this thickness dependence strongly favors magnetoelastic anisotropy over W/Au/Fe interface anisotropy as driving force for the $[1\bar{1}0]$ easy axis.

These structural changes have a strong influence on the magnetization as indicated by the asymmetry. In the bcc ps state (<2 ML) the atomic packing density is much lower than in the thicker Fe films with nearly bulk periodicity (14.12×10^{14} vs 17.21×10^{14} atoms/cm^2). This leads to a larger magnetic moment evident in the large asymmetry at 2 ML. The rapid increase in the asymmetry between 1.6 and 2 ML cannot be assigned to the 0.4 ML but indicates transformation of part or all of the existing material into the high spin state.

The transition to the bulklike bcc layer with higher packing density reduces the magnetic moment resulting in the observed decrease in the asymmetry between 2 and 4 ML. At 4 ML the packing density approaches that of Fe in the bulk so that the subsequent nearly linear increase in the asymmetry can be attributed to the increase in the number of (constant) magnetic moments, keeping in mind that there is no one-to-one relation between the magnitude of asymmetry and the magnetization

The relative magnetic moment in the ps Fe layer compared to that in the Fe layer with nearly bulk periodicity may be estimated if a nearly 1:1 correspondence between asymmetry and magnetization is assumed and if possible complications by diffraction effects are neglected. Taking damping by inelastic scattering into account the asymmetry signal from a N ML thick film is given by $I_N=I_1\times[1-\exp(-Nd/\lambda)]/[1-\exp(-d/\lambda)]$, with I_1 as the signal from 1 ML, the ML thickness $d=2$ Å, and the IMFP $\lambda=4$ Å. With these numbers $I_{1\mathrm{bcc}}=I_6/2.415$ in the bulklike bcc ML. From the 2 ML asymmetry value one obtains in the same manner $I_{1\mathrm{ps}}=I_2/1.606$. With the data of Fig. 4, $I_2=0.05$ and $I_6=0.069$, one obtains $I_{1\mathrm{ps}}/I_{1\mathrm{bcc}}=1.09$. Here it was assumed that the first 2 Fe MLs are in the high spin state at a thickness of 2 ML. If the first ML would remain nonmagnetic at 2 ML thickness, then this ratio would be 1.69. If asymmetry and magnetization were proportional, then this value can be excluded because it would give an abnormally high magnetic moment for the high spin state compared to that of bulk Fe. Even the moment enhancement by the Au layers between the 2 ML Fe are sandwiched[38] cannot explain such a large value. Within the framework of these assumptions it thus follows that the first 2 MLs transform into the high spin state between 1.6 and 2 ML.

Between 6 and 7 ML nanofaceting starts leading to a roof structure along the [001] direction, Fig. 10(d). This causes a shape anisotropy along the [001] direction and the rotation of **M** toward [001]. The faceting increases the roughness of the surface so that the simultaneous decrease in the asymmetry may be attributed to a decrease in the magnetization due to demagnetization caused by the roughness (dipolar magnetic surface anisotropy[39]). The asymmetry reaches a constant value at about 10 ML, which in the framework of this hypothesis would imply that the roughness becomes stationary. On the other hand, kinetic faceting is known to increase like the square root of the thickness, in particular also during the growth of Fe films.[32,40] This may not be the case in the presence of a Au overlayer, which certainly will influence the surface kinetics. An indication of such an influence is the delayed onset of faceting at 7 ML compared to 1–2 ML on the clean Fe surface.[32] In the whole Fe thickness range magnetocrystalline anisotropy favors the [001] direction as the easy axis. However, its contribution to the total magnetic anisotropy in the ultrathin thickness range is usually negligible.[11]

Having discussed the general trend of the magnetization as a function of film thickness and its relation to the structure of the film, some comments have to be made yet about the evolution of the magnetization in the individual domains. Although the magnitude of the magnetization is very similar in all domains—except for the lower values on the step bunch—the direction of the magnetization varies considerably from domain to domain so that on the micron scale **M** is laterally noncollinear in contrast to Fe layers grown on W(110) and thick Au(111) layers on W(110). This is particularly evident in the subdomains elongated in the $[1\bar{1}0]$ directions [Fig. 1(m)]. The angle of the magnetization between them depends upon thickness and can reach as much as 60°. There is no microstructural explanation for this phenomenon because the long axes of the domains are perpendicular to the few atomic steps below these subdomains. Another hint at noncollinearity is the observation of subdomains with constant shape and thickness-dependent weak intensity. This could possibly be attributed to weak noncollinearity perpendicular to the surface. Fe is known to have a strong tendency to noncollinearity (see, e.g., Refs. 41–46). Noncollinearity is usually suppressed by the spin-aligning effects of the various anisotropies that are usually present in thin film systems. Noncollinear magnetism in Fe films has recently also been suggested based on nuclear resonant scattering from ^{57}Fe.[47] Effects of the kind seen here in Fe layers have never been observed in Co films, in which noncollinear magnetism is not expected.

It is interesting to compare the results obtained here with the magnetism and structure of Fe films on Cu(111) surfaces. Contrary to Au(111), 2 ML Au on W(110) and W(110) sur-

faces the misfit between Cu and fcc (111) Fe is small (a_{Cu}=3.615 Å vs a_{Fe}=3.515 Å). Therefore, one would expect initial pseudomorphic fcc growth. This has indeed been observed in LEED (Refs. 48 and 49) up to a thickness of 2.3–3 ML at which a transition to bcc growth occurs similar to the transition seen here at 2 ML. Simultaneously, in-plane magnetization appears. STM shows a more complicated picture with bcc regions already appearing at 1 ML on top of multilayer fcc islands. This is similar to the coexistence of ps Fe and narrow bcc-like Fe nanocrystals indicated by the LEED patterns in this work though the formation mechanism is likely different. Growth starts with bilayer islands, which at 1 ML nominal thickness have already linear dimensions of 100 Å. Islands of this size should give LEED spots and not the diffuse streaks observed here on 2 ML Au/W. A more detailed STM study,[50] which compares growth at 300 and 80 K, suggests a possible mechanism for the initial growth of Fe on 2 ML Au/W. On Cu(111) elongated features with bcc-like structure are present at 80 K already at 1 ML. Similar features appear in films deposited by pulsed laser deposition at 220 K during the transition from fcc to bcc structure.[48,49] In both cases mobility is significantly reduced and nucleation rate increased compared to the thermal deposition at room temperature used in the present study.

A similar situation occurs very likely also in the initial growth of Fe on 2 ML Au/W. The initial growth of large monolayer islands of Fe on Au(111)[13,14] is impeded by the Au that is expelled from the compressed Au double layer during the transition to the ps structure. With further increasing Fe thickness more Au is moving to the surface leaving only one Au monolayer behind and one on top of the Fe layer. The high energy in the fine-grained layer finally leads to recrystallization and expulsion of the Au still present at the Fe grain boundaries. Though speculative, this scenario gives a reasonable interpretation of the observations and their difference from the apparently similar system Fe/Cu(111).

V. SUMMARY

The present study shows that a Au double layer on W(110) uncouples the influence of the substrate on a Fe layer grown on it sufficiently so that structural changes in the film, involving also the redistribution of Au, are reflected in a complicated dependence of the magnetization upon film thickness. The structural changes include partial segregation of Au onto the growing Fe layer, transition from a mixture of ps Fe and fine-grained bulklike bcc Fe to larger bulklike bcc Fe crystallites with interfacial dislocation networks, and finally faceting. These structural changes cause corresponding changes in the magnetization direction via the thickness-dependent competition of interface anisotropies, magnetoelastic anisotropy, and dipolar surface anisotropy. The details of the domain structure suggest this competition suppresses spin-aligning anisotropies sufficiently to reveal the natural tendency of Fe to noncollinearity.

ACKNOWLEDGMENTS

This work was supported in part by the National Science Foundation (Grant No. DMR-9818296) and by the Office of Naval Research [Grant No. N000140210922 (UPAS)]. R.Z. also acknowledges support by the Polish Ministry of Science and Higher Education under Grant No. N202 159 32/4302.

[1] C. A. F. Vaz, J. A. C. Bland, and G. Lauhoff, Rep. Prog. Phys. **71**, 056501 (2008) and references therein.
[2] D. Sander, W. Pan, S. Ouazi, J. Kirschner, W. Meyer, M. Krause, S. Müller, L. Hammer, and K. Heinz, Phys. Rev. Lett. **93**, 247203 (2004) and references therein.
[3] U. Gradmann and G. Waller, Surf. Sci. **116**, 539 (1982).
[4] P. J. Berlowitz, J.-W. He, and D. W. Goodman, Surf. Sci. **231**, 315 (1990).
[5] H. Bethge, D. Heuer, Ch. Jensen, K. Reshöft, and U. Köhler, Surf. Sci. **331-333**, 878 (1995).
[6] R. Popescu, H. L. Meyerheim, D. Sander, J. Kirschner, P. Steadman, O. Robach, and S. Ferrer, Phys. Rev. B **68**, 155421 (2003).
[7] N. Weber, K. Wagner, H. J. Elmers, J. Hauschild, and U. Gradmann, Phys. Rev. B **55**, 14121 (1997).
[8] U. Gradmann, J. Korecki, and G. Waller, Appl. Phys. A: Mater. Sci. Process. **39**, 101 (1986).
[9] H. J. Elmers and U. Gradmann, Appl. Phys. A: Mater. Sci. Process. **51**, 255 (1990).
[10] I.-G. Baek, H. G. Lee, H.-J. Kim, and E. Vescovo, Phys. Rev. B **67**, 075401 (2003).
[11] D. Sander, Rep. Prog. Phys. **62**, 809 (1999).
[12] G. Honjo, K. Takayanagi, K. Kobayashi, and K. Yagi, J. Cryst. Growth **42**, 98 (1977).
[13] B. Voigtländer, G. Meyer, and N. M. Amer, Surf. Sci. Lett. **255**, L529 (1991).
[14] J. A. Stroscio, D. T. Pierce, R. A. Dragoset, and P. N. First, J. Vac. Sci. Technol. A **10**, 1981 (1992).
[15] J. Xu, M. A. Howson, P. Hucknall, B. J. Hickey, R. Venkataraman, C. Hammond, M. J. Walker, and D. Greig, J. Appl. Phys. **81**, 3908 (1997).
[16] P. Ohresser, N. B. Brookes, S. Padovani, F. Scheurer, and H. Bulou, Phys. Rev. B **64**, 104429 (2001).
[17] O. Toulemonde, V. Petrov, A. Nait Abdi, and J. P. Bucher, J. Appl. Phys. **95**, 6565 (2004).
[18] P. Gueguen, M. Cahoreau, and M. Gillet, Thin Solid Films **16**, 27 (1973).
[19] D. T. Dekadjevi, B. J. Hickey, S. Brown, T. P. A. Hase, B. D. Fulthorpe, and B. K. Tanner, Phys. Rev. B **71**, 054108 (2005).
[20] G. Lugert and G. Bayreuther, Thin Solid Films **175**, 311 (1989).
[21] G. Lugert, W. Robl, L. Pfau, M. Brockmann, and G. Bayreuther, J. Magn. Magn. Mater. **121**, 498 (1993).
[22] C. Chappert, P. Bruno, B. Bartenlian, P. Beauvillain, A. Bounouh, R. Megy, and P. Veillet, J. Magn. Magn. Mater. **148**, 165 (1995).
[23] H. J. Elmers and U. Gradmann, Surf. Sci. **304**, 201 (1994).
[24] R. Zdyb and E. Bauer, Phys. Rev. B **67**, 134420 (2003).

[25] R. Zdyb, A. Pavlovska, and E. Bauer, J. Phys.: Condens. Matter **21**, 314012 (2009).
[26] E. Bauer and T. Schmidt, in *High-Resolution Imaging and Spectroscopy of Materials*, edited by F. Ernst and M. Ruehle (Springer, Berlin, 2003), p. 363.
[27] A. Locatelli, L. Aballe, T. O. Menteş, M. Kiskinova, and E. Bauer, Surf. Interface Anal. **38**, 1554 (2006).
[28] E. Bauer, in *Magnetic Microscopy of Nanostructures*, edited by H. Hopster and H. P. Oepen (Springer, Berlin, 2005), p. 111; *Modern Techniques for Characterizing Magnetic Materials*, edited by Y. Zhu (Kluwer, Boston, 2005), p. 361.
[29] T. Duden and E. Bauer, Rev. Sci. Instrum. **66**, 2861 (1995).
[30] E. Bauer, H. Poppa, G. Todd, and P. R. Davis, J. Appl. Phys. **48**, 3773 (1977).
[31] A. B. Greninger and A. R. Troiano, Trans. AIME **185**, 590 (1949).
[32] M. Albrecht, H. Fritzsche, and U. Gradmann, Surf. Sci. **294**, 1 (1993).
[33] R. Zdyb, T. O. Menteş, A. Locatelli, M. A. Niño, and E. Bauer (unpublished).
[34] R. Zdyb (unpublished).
[35] H. C. Siegmann, Surf. Sci. **307-309**, 1076 (1994).
[36] J. Hong and D. L. Mills, Phys. Rev. B **62**, 5589 (2000).
[37] H. Fritzsche, H. J. Elmers, and U. Gradmann, J. Magn. Magn. Mater. **135**, 343 (1994).
[38] L. Szunyogh, B. Újfalussy, and P. Weinberger, Phys. Rev. B **51**, 9552 (1995).
[39] P. Bruno, J. Appl. Phys. **64**, 3153 (1988).
[40] M. Albrecht, T. Furubayashi, M. Przybylski, and U. Gradmann, J. Magn. Magn. Mater. **113**, 207 (1992).
[41] V. P. Antropov, M. I. Katsnelson, M. van Schilfgaarde, and B. N. Harmon, Phys. Rev. Lett. **75**, 729 (1995).
[42] L. M. Sandratskii, Adv. Phys. **47**, 91 (1998).
[43] D. Spišák and J. Hafner, Phys. Rev. B **67**, 134434 (2003).
[44] A. J. Freeman, K. Nakamura, and T. Ito, J. Magn. Magn. Mater. **272-276**, 1122 (2004).
[45] L. Tsetseris, Phys. Rev. B **72**, 012411 (2005).
[46] K. Nakamura, N. Mizuno, T. Akiyama, T. Ito, and A. J. Freeman, J. Appl. Phys. **101**, 09G521 (2007).
[47] T. Ślęzak, S. Stankov, M. Zając, M. Ślęzak, K. Matlak, W. Karaś, N. Spiridis, B. Laenens, N. Planckaert, M. Rennhofer, K. Freindl, D. Wilgocka-Ślęzak, R. Rüffer, and J. Korecki, Mater. Sci. (Poland) **26**, 885 (2008).
[48] J. Shen, M. Klaua, P. Ohresser, H. Jenniches, J. Barthel, Ch. V. Mohan, and J. Kirschner, Phys. Rev. B **56**, 11134 (1997).
[49] P. Ohresser, J. Shen, J. Barthel, M. Zheng, Ch. V. Mohan, M. Klaua, and J. Kirschner, Phys. Rev. B **59**, 3696 (1999), and references therein.
[50] A. Biedermann, W. Rupp, M. Schmid, and P. Varga, Phys. Rev. B **73**, 165418 (2006).